Intrinsic Disorder Mediates the Diverse Cell Cycle Regulatory Functions of the Cyclin-dependent kinase Inhibitor, p21^{Cip1}

Yuefeng Wang[1], John C. Fisher[1,4,5], Rose Matthew[2], Li Ou[1], Steve Otieno[1], Jack Sublett[3], Limin Xiao[1], Jianhan Chen[7], Martine F. Roussel[2,4,6], and Richard W. Kriwacki[1,4,6*]

[1]Departments of Structural Biology, [2]Genetics and Tumor Cell Biology, and [3]Infectious Diseases, St. Jude Children's Research Hospital, Memphis, TN, USA; [4]Integrated Program in Biomedical Sciences, [5]College of Medicine, and [6]Department of Molecular Sciences, University of Tennessee Health Science Center, Memphis, TN 38163, USA; and [7]Department of Biochemistry, Kansas State University, Manhattan, KS 66506, USA.

[*]Corresponding author: Department of Structural Biology, Mail Stop 311, St. Jude Children's Research Hospital, 262 Danny Thomas Place, Memphis, TN 38105-3678, USA.
Tel: 901-595-3290; Fax: 901-595-3032; E-mail: richard.kriwacki@stjude.org.

Keywords: cell cycle, cyclin, cyclin-dependent kinase inhibitor, binding diversity, solution NMR, kinase assay.

Supplementary Methods

Preparation of peptides

The following peptides corresponding to wild-type and variant sub-domains of p21-KID were prepared by solid-phase synthesis by the Hartwell Center for Bioinformatics and Biotechnology at St. Jude Children's Research Hospital: D1, N-GSKACRRLFGPVD-C; wild-type LH, N-DSEQLSRDCDALMAGCIQEARER-C; LH_{+3}, N-DSEQLSRDCDALMAGCIQEARERALR-C; LH_{-3}, N-DSEQLSRDCDALMAGCIQEA-C, and D2, N-WNFDFVTETPLEGDFAWERVRGLGLPKLYLPTG-C. All peptides were purified by high-performance liquid chromatography and their identities confirmed by mass spectrometry.

Isothermal Calorimetry (ITC) Experiments

ITC experiments were performed using an Auto ITC-200 (GE Healthcare, Piscataway, NJ) at 25 ℃. In all the experiments, p21 peptides were titr ated, through 19 individual, 2 µL injections, into a solution of the Cdk2/Cyclin A complex in the calorimeter cell (cell volume, 200 µL). For the titration D1 into Cdk2/Cyclin A, a 65 µM p21-D1 solution was in the syringe and a 5 µM Cdk2/cyclin A solution was in the cell; the sample buffer (for both syringe and cell solutions) was composed of 20 mM HEPES pH 7.5, 300 mM NaCl, 1 mM TCEP-HCl. For the remainder of ITC experiments, the buffer above was supplemented with 5% DMSO and the concentration of Cdk2/Cyclin A was 90 µM. The concentrations of wild-type LH, LH_{+3} and LH_{-3} were 1 mM while the concentration of D2 was 600 µM. The appropriate control experiments were performed to determine the magnitude of the heats of dilution, including buffer into Cdk2/cyclin A and syringe polypeptide solutions into buffer; these heats were all negligible. These included buffer into Cdk2/cyclin A and syringe polypeptide solutions into buffer. The raw titration data were analyzed using Origin 7.0 software (OriginLab, Northampton, MA) with the 1:1 binding model.

Computations performed to estimate the free energy cost of substituting four Glu residues in p27-D2 with the corresponding residues in p21-D2

Brief summary. Atomistic implicit solvent[1,2] free energy simulations estimated that substituting four Glu residues at positions 75, 78, 80 and 86 within p27-D2 with the corresponding residues of p21-D2 (Ala, Arg, Arg, and Lys, respectively) could cost over +15 kcal/mol, within the structural context of the p27/Cdk2/cyclin A ternary complex (see Suppl. Fig. 4a). This estimation mainly reflects the cost due to electrostatic repulsion due to introduction of positive charges (from p21-D2) at an interface with Cdk2 which exhibits strong positive electrostatic potential (Suppl. Fig. 4a and b). Clearly, this is a crude estimate and we acknowledge that mutual structural adjustments would occur when p21 binds to Cdk2/cyclin A. The results from ITC show that the difference in ΔG values for p21-D2 (-7.2 kcal mol^{-1}) and p27-D2 (-9.8 kcal mol^{-1})[3] binding to Cdk2/cyclin A is +2.6 kcal mol^{-1}, clearly indicating that structural accommodation of repulsive electrostatic interactions occurs. Nonetheless, the free energy estimation supports our hypothesis that electrostatic forces are likely the main cause of the much weaker binding of the p21-D2 sub-domain to Cdk2/cyclin A.

Details of the free energy calculations. Atomistic simulations were carried out to estimate the free energy cost of substituting four Glu residues in the D2 sub-domain of p27 with the corresponding residues of p21, as noted above. Due to the lack of high-resolution structural information for the p21/Cdk2/cyclin A ternary complex, the free energy cost was estimated in the structural context of the p27/Cdk2/cyclin A ternary complex (PDB: 1JSU[4]). Protein backbone atoms were constrained to their initial positions throughout the simulations (in complex and in isolation), and only side chains were allowed to move due to the residue substitutions. Given the size and complexity of the system, several approximations were made to further reduce the computational cost and enable estimation of free energies. First, solvent effects were described

using implicit solvent. Two previously optimized generalized-Born protein force fields were used, including GBSW[2,5] and GBMV2[1,6]. The key difference between GBSW and GBMV is in the description of the solvent-solute boundary: van der Waals-like surface in GBSW and molecular surface in GBMV. Using both implicit solvent models provided an opportunity to detect the potential protein force field dependence of the free energy estimation. Second, a reduced molecular construct was used wherein only portions of Cdk2/cyclin A that are directly involved in interactions with p27-D2 were included (see Suppl. Fig. 4c). The C-terminal portion of the LH sub-domain was also included in the construct due to its extensive interaction with the D2 sub-domain.

All simulations and subsequent analyses were carried out using CHARMM[7,8]. The molecular systems were first equilibrated for 100 ps using Langevin dynamics at 300 K. The time step was 2 fs with GBSW and this was reduced to 1 fs for GBMV (due to elevated numerical instability of the GBMV model). After equilibration, 1.0 ns production simulations were performed. As shown in Suppl. Fig. 4d, potential energies quickly stabilized within the 1.0 ns simulation time scale. To estimate the free energy of substituting the four Glu residues in p27-D2, four simulations were required: wild-type p27 in isolation (free-wt) and in complex with Cdk2 (cmplx-wt), and substituted p27 in isolation (free-mut) and in complex (cmplx-mut). Upon completion of these computations, the free energy cost of the substitutions was estimated as given in Eq. 1, below.

$$\Delta\Delta G \sim \left\langle E_{\text{cmplx}-\text{mut}} \right\rangle - \left\langle E_{\text{cmplx}-\text{wt}} \right\rangle - \left(\left\langle E_{\text{free}-\text{mut}} \right\rangle - \left\langle E_{\text{free}-\text{wt}} \right\rangle \right) \qquad (\mathbf{1})$$

In Eq. 1, <> denotes the ensemble average over the last 500 ps of the production computations. The entire free energy computation was repeated three times to estimate the uncertainty, as summarized in Supplementary Table 2.

Cell culture, virus infection, cell cycle analysis, immunoblotting and immunoprecipitation analyses

NIH 3T3 mouse embryo fibroblasts were grown in Dulbecco's modified Eagle's medium supplemented with 10% fetal bovine serum, L-glumatine and penicillin/streptomycin[67]. Wild type and LH sub-domain p21 variants with an N-terminal HA tag were expressed from the MSCV retrovirus vectors that express the gene for green fluorescent protein (GFP) in *cis* by virtue of an internal ribosome entry site[44]. 2 x10^5 cells per 100 mm plate of exponentially growing NIH 3T3 cells were infected with 2 ml of high titer mouse recombinant viruses generated in 293T cells as described previously[44]. 32 hours post-infection, cell cycle analysis was performed. Samples containing 10^6 cells were centrifuged and resuspended in 1 ml of propidium iodide staining solution (0.05 mg/ml propidium iodide, 0.1 % sodium citrate, 0.1% Triton X-100). Immediately prior to analysis by flow cytometry, each sample was treated at room temperature with DNAse-free RNase (Calbiochem) at a final concentration of 5 μg/ml for 30 minutes, and filtered through 40 μm nylon mesh. Fluorescence of wavelength 563-607 nm emitted from propidium iodide-DNA complexes was measured from approximately 20,000 cells with a FACS Calibur flow cytometer (BD Biosciences). The percentages of cells within the G_1/G_0, S, and G_2/M phases of the cell cycle were determined by analysis with the computer program ModFit (Verity Software House).

Whole cell lysates from retroviral infected cells (described above) were prepared from cells sorted based on GFP expression, pelleted, and resuspended in M-PER protein extraction reagent (Pierce) supplemented with 10 μM EDTA and protease inhibitors. Lysates were incubated at 4 ℃ with gentle shaking and centrifug ed at 16,000 x g at 4 ℃ for 20 minutes. The amount of total protein from each supernatant fraction was determined by BCA assay (Pierce). Lysates were adjusted with M-PER reagent to equalize protein concentrations. For protein expression analysis, 10 μg of protein was loaded per lane and separated using the Criterion XT

4-12% gel system with 1X MOPS buffer at 200 V. Proteins were transferred to nitrocellulose using standard blotting conditions, blocked with 1% BSA in TBS (blocking buffer), and primary antibodies (in blocking buffer: anti-HA clone 3F10 (Roche) 1:1000 and anti-actin clone C4 (ImmunO) 1:5000) were incubated for one hour at room temperature. Horse radish peroxidase-conjugated, goat anti-rat secondary antibody (Santa Cruz) (1:5000 in blocking buffer) was incubated at room temperature for 45 min. before standard enhanced chemiluminescence detection using SuperSignal West Pico Chemiluminescent Substrate (Pierce) and an ImageQuant LAS 4000 Biomolecular Imager (Fugi).

HA-fusion proteins were immunoprecipitated using the ProFound HA Tag IP kit (Pierce) per the manufacturer's protocol. Briefly, 10 μg of agarose-conjugated anti-HA antibody was added to 250 μl of each cell whole lysate from retroviral infected cells (270 μg total protein) and incubated at 4 ℃ overnight. Cell lysates were remo ved after centrifugation, and the agarose-conjugated anti-HA antibody was washed three times with Tris buffered saline supplemented with 0.05 % Tween-20 (Sigma). Proteins were eluted by adding 25 μl of 2X non-reducing sample buffer to the agarose-conjugated HA antibody, incubated for 10 minutes at room temperature, and centrifuged to separate the eluted proteins from the agarose-conjugated HA antibody. 3 μl of 1 M DTT was added to each eluent, and the eluted proteins were boiled for 5 minutes prior to separation by SDS-PAGE and transferred to nitrocellulose as described above. HA-fusion proteins were detected as described above. Cdk2 and Cdk4 were detected using rabbit anti-sera as previously described[68]. Cdk1 was detected using mouse anti-Cdc2 clone b4 (Santa Cruz, 1:1000) in 5% non-fat milk.

References for Supplementary Methods

1. Chen, J.H. Effective Approximation of Molecular Volume Using Atom-Centered Dielectric Functions in Generalized Born Models. *Journal of Chemical Theory and Computation* **6**, 2790-2803 (2010).

2. Chen, J.H., Im, W.P. & Brooks, C.L. Balancing solvation and intramolecular interactions: Toward a consistent generalized born force field. *Journal of the American Chemical Society* **128**, 3728-3736 (2006).
3. Lacy, E.R. et al. p27 binds cyclin-CDK complexes through a sequential mechanism involving binding-induced protein folding. *Nat. Struct. Mol. Biol.* **11**, 358-364 (2004).
4. Russo, A.A., Jeffrey, P.D., Patten, A.K., Massague, J. & Pavletich, N.P. Crystal structure of the p27(Kip1) cyclin-dependent-kinase inhibitor bound to the cyclin A Cdk2 complex. *Nature* **382**, 325-331 (1996).
5. Im, W.P., Lee, M.S. & Brooks, C.L. Generalized born model with a simple smoothing function. *Journal of Computational Chemistry* **24**, 1691-1702 (2003).
6. Lee, M.S., Salsbury, F.R. & Brooks, C.L. Novel generalized Born methods. *Journal of Chemical Physics* **116**, 10606-10614 (2002).
7. Brooks, B.R. et al. Charmm - a Program for Macromolecular Energy, Minimization, and Dynamics Calculations. *Journal of Computational Chemistry* **4**, 187-217 (1983).
8. Brooks, B.R. et al. CHARMM: The Biomolecular Simulation Program. *Journal of Computational Chemistry* **30**, 1545-1614 (2009).
9. Im, W., Beglov, D. & Roux, B. Continuum solvation model: Electrostatic forces from numerical solutions to the Poisson-Boltzmann equation. *Comput. Phys. Comm.* **111**, 59-75 (1998).

Supplementary Results

Supplementary Table 1. Thermodynamic parameters determined by ITC at 25°C for p21 sub-domain peptides binding to Cdk2/cyclin A. Refer to Supplementary Fig. 3 for the corresponding raw titration data.

Interaction	**K_d (nM)**	**ΔG [a] (kcal mol^{-1})**	**ΔH (kcal mol^{-1})**	**-TΔS [b] (kcal mol^{-1})**
D1 + Cdk2/cyclin A	60.6	-9.8	-18.2	+8.4
wt LH + Cdk2/cyclin A	>90,000 [c]	>-5.5 [d]	0	>-5.5
LH_{+3} + Cdk2/cyclin A	>90,000 [c]	>-5.5 [d]	0	>-5.5
LH_{-3} + Cdk2/cyclin A	>90,000 [c]	>-5.5 [d]	0	>-5.5
D2 + Cdk2/cyclin A	5300	-7.2	-11.0	+3.8

The stoichiometry of binding (n) was determined to be 1.0, with experimental error less than 10% for those experiments in which the stoichiometry could be determined.

[a] Calculated with the equation $\Delta G = -RT \ln(1/K_d)$

[b] Calculated with the equation $-T\Delta S = \Delta G - \Delta H$

[c] This value is an approximate lower limit for K_d based on the failure to observe significant heat of binding under the conditions of the experiment.

[d] These values are approximate lower limits for ΔG and -TΔS based on the limiting K_d value and the observation that $\Delta H \approx 0$.

Supplementary Table 2. Free energy difference (for binding to Cdk2/cyclin A) of substituting four Glu residues in the D2 sub-domain of p27 with the corresponding residues of p21.

	Free energy difference due to residue substitutions (kcal mol^{-1})	
Computation #	**GBSW**	**GBMV**
Run 1	17.24	12.72
Run 2	13.48	29.65
Run 3	15.63	10.92
Average	15.45 ± 1.54	17.76 ± 8.44

Supplementary Figure 1. 2D ^{1}H-^{15}N TROSY spectra of ternary complexes show that the two sub-domain LH variants, p21-KID -LH_{-3} (**b**) and p21-KID -LH_{+3} (**d**), bind to the Cdk2 and cyclin A subunits of the Cdk2/cyclin A complex in a manner very similar to that observed for wild-type p21-KID (**c**). The sequences for p21-KID, p21-KID-LH_{-3} and p21-KID-LH_{+3} are shown in panel **a**. Resonances for residues of the $^{2}H/^{15}N$-labeled p21-KID constructs within sub-domain D1 that bind cyclin A (labeled with blue letters) and within sub-domain D2 that bind to Cdk2 (labeled with green letters) exhibit similar chemical shift values in the three spectra.

Supplementary Figure 2. Thermal denaturation curves based on measurements of CD ellipticity at 222 nm as a function of temperature (25 to 93 ℃) for Cdk2/cyclin A (black "X" symbols and line), p21-KID/Cdk2/cyclin A (red diamonds and line), p21-KID-LH_{+3}/Cdk2/cyclin A (blue triangles and line), and p21-KID-LH_{-3}/Cdk2/cyclin A (green circles and line). Raw ellipticity values were converted to fraction (of proteins) unfolded for plotting.

Supplementary Figure 3. Raw ITC data and isotherms for individual p21 sub-domains titrated into Cdk2/cyclin A. The titrants were (**a**) D1, (**b**) wild-type LH, (**c**) LH_{+3}, (**d**) LH_{-3} and (**e**) D2.

Supplementary Figure 4. Analysis of electrostatic contributions to interactions between sub-domains D2 of p27 (p27-D2) and p21 (p21-D2) and the Cdk2/cyclin A complex. **(a)** Structure of p27-KID bound to Cdk2/cyclin A (PDB: 1JSU). The four Glu residues of p27-D2 (illustrated as a green ribbon) that are substituted with basic and neutral residues in p21-D2 are indicated. The Cdk2/cyclin A complex is shown in molecular surface, and colored based on the surface electrostatic potential calculated in the absence of p27 using the PBEQ module[9] in CHARMM[8] (blue: positive; red: negative). (**b**) Expanded view of boxed region in (**a**). (**c**) Truncated portions

of p27-KID and Cdk2 used for MD and potential energy computations. Residues 52-93 of p27 [p27(52-93)] and residues 13-198 of Cdk2 were included in the computations. The p27 D2 sub-domain is colored in green and Cdk2 colored in gray. The side chains of the four Glu residues that are substituted in p21-D2 (Glu75 to Ala, Glu78 to Arg, Glu80 to Arg, and Glu86 to Lys) are illustrated as sticks. (**d**) Representative time traces of potential energies of wild-type p27(52-93) and p27(52-93) with four Glu residues substituted as above noted in (**c**) (p27-mut) in complex with Cdk2 (labeled p27/Cdk2 and p27-mut/Cdk2) and in isolation (labeled free p27 and free p27-mut) during 1 ns production simulations using GBSW implicit solvent. As can be observed, energies of all simulated constructs stabilized rapidly and did not drift significantly during the 1.0 ns production simulations.

Supplementary Figure 5. Inhibition of the kinase activity of a panel of Cdk/cyclin complexes by p21-KID (circles), p21-KID-LH$_{+3}$ (squares) and p21-KID-LH$_{-3}$ (triangles); inhibition of Cdk1/cyclin B1 (**a**), Cdk2/cyclin A (**b**), Cdk4/cyclin D1 (**c**), and Cdk6/Cyclin D1 (**d**). The percentage of kinase activity toward Rb^{C} at each concentration was fitted to a log ([inhibitor]) *versus* response curve as described under Materials and Methods. (**e**) Table of IC$_{50}$ values for inhibition of the different Cdk/cyclin complexes by wild-type p21-KID and the sub-domain LH variants illustrated in panels **a**-**d**.

Supplementary Figure 6. Elongation or truncation of sub-domain LH within p21 significantly influences cell cycle regulation. Cell cycle analysis of NIH 3T3 cells expressing (**a**) GFP only or (**b**) GFP and p19^{Ink4d}, (**c**) p21-LH$_{-3}$, (**d**) p21, or (**e**) p21-LH$_{+3}$, as indicated. Illustrated here are representative data from a single experiment; the summary data reported in Table 2 represent averages of multiple experiments, as indicated.

Supplementary Figure 7. The HA-tagged p21 constructs, as indicated in the figure, were expressed at equivalent levels in mouse fibroblast cells. The levels of the indicated retrovirally expressed, HA-tagged p21 constructs were determined by immunoblot analysis of total cell lysates from NIH 3T3 cells. Cells infected with retroviral vectors expressing only GFP, and GFP and $p19^{Ink4d}$, both of which lack an HA tag, were used as negative controls. Equal total protein loading was confirmed by immunoblot analysis for actin.

Supplementary Figure 8. Fill-size images for immunoblot analysis of HA-tagged p21 constructs expressed in NIH 3T3 cells as illustrated in Supplementary Fig. 7.

Supplementary Figure 9. Endogenous Cdk1, Cdk2 and Cdk4 were expressed at similar levels in NIH 3T3 fibroblast cells infected with retroviruses expressing the indicated HA-tagged p21 constructs. The levels of the indicated Cdks were determined by immunoblot analysis of total cell lysates from NIH 3T3 cells as described under Materials and Methods.

Supplementary Figure 10. Full-size image for results of immunoprecipitation of HA-tagged proteins from NIH 3T3 cell lysates followed by SDS-PAGE and immunoblotting using antibodies for Cdk1, Cdk2 and Cdk4, illustrated in the main text as Fig. 4b.

Supplementary Figure 11. Full-size image for results of immunoblotting using an antibody for the HA tag for the NIH 3T3 cell lysates illustrated in the main text as Fig. 4c. From left to right, isolated HA-tagged GFP protein (positive control), and lysates from cells expressing GFP only (GFP, negative control) or GFP and HA-tagged p21-LH_{-3} (p21-LH_{-3}), HA-tagged wild-type p21 (p21) or HA-tagged p21-LH_{+3} (p21-LH_{+3}).

Supplementary Figure 1

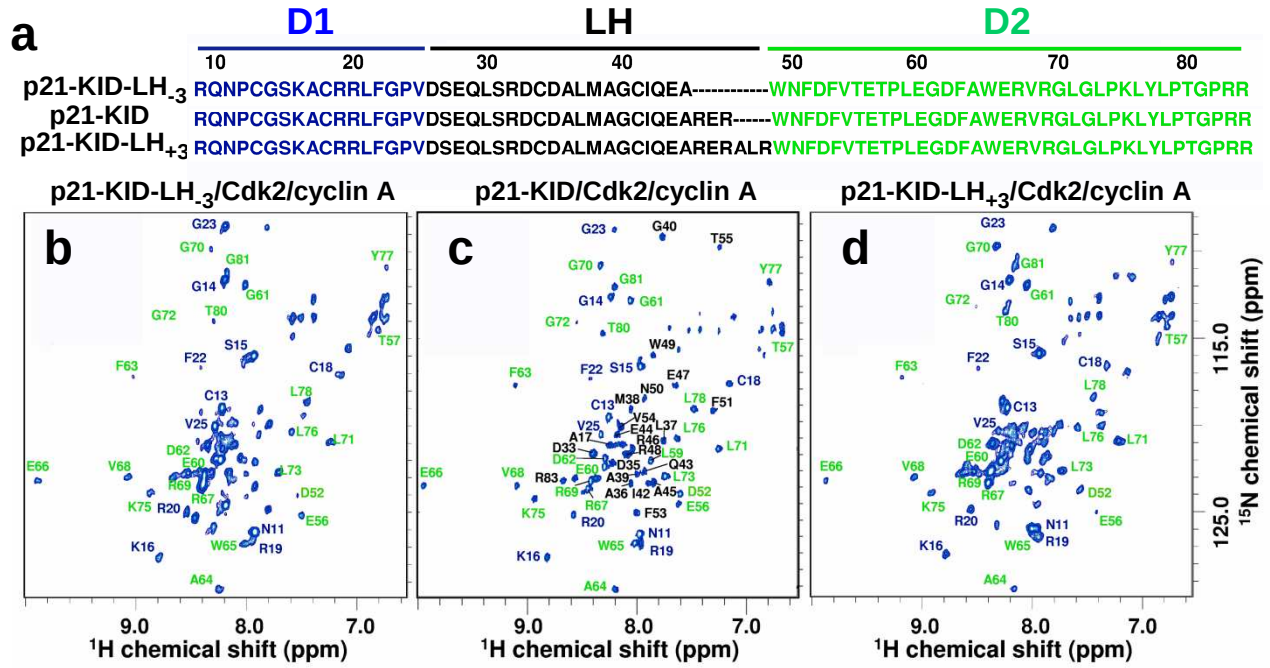

Supplementary Figure 2

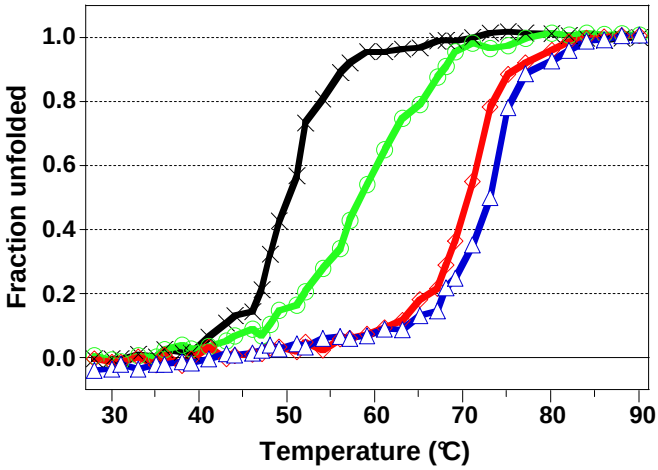

Supplementary Figure 3

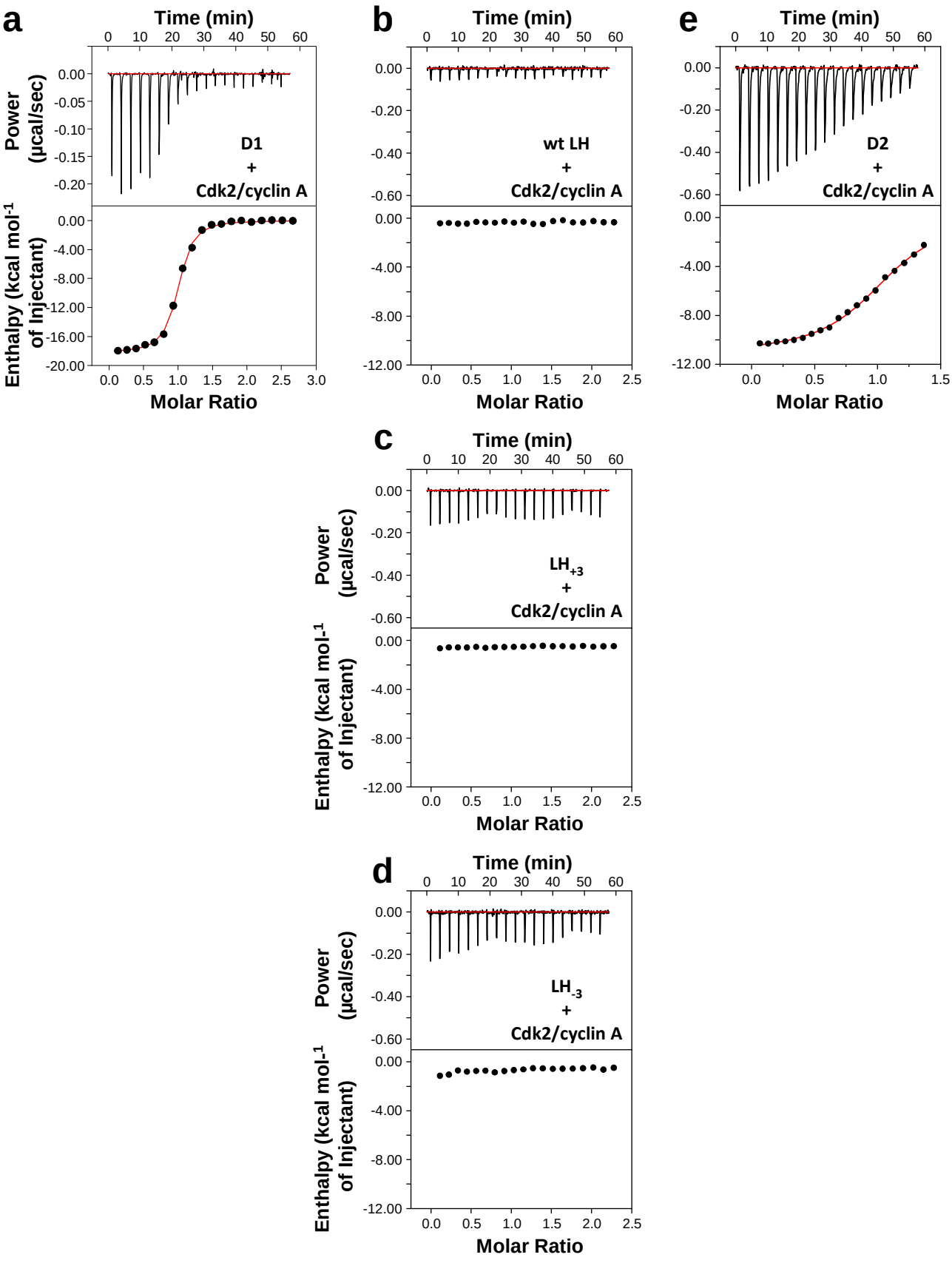

Supplementary Figure 4

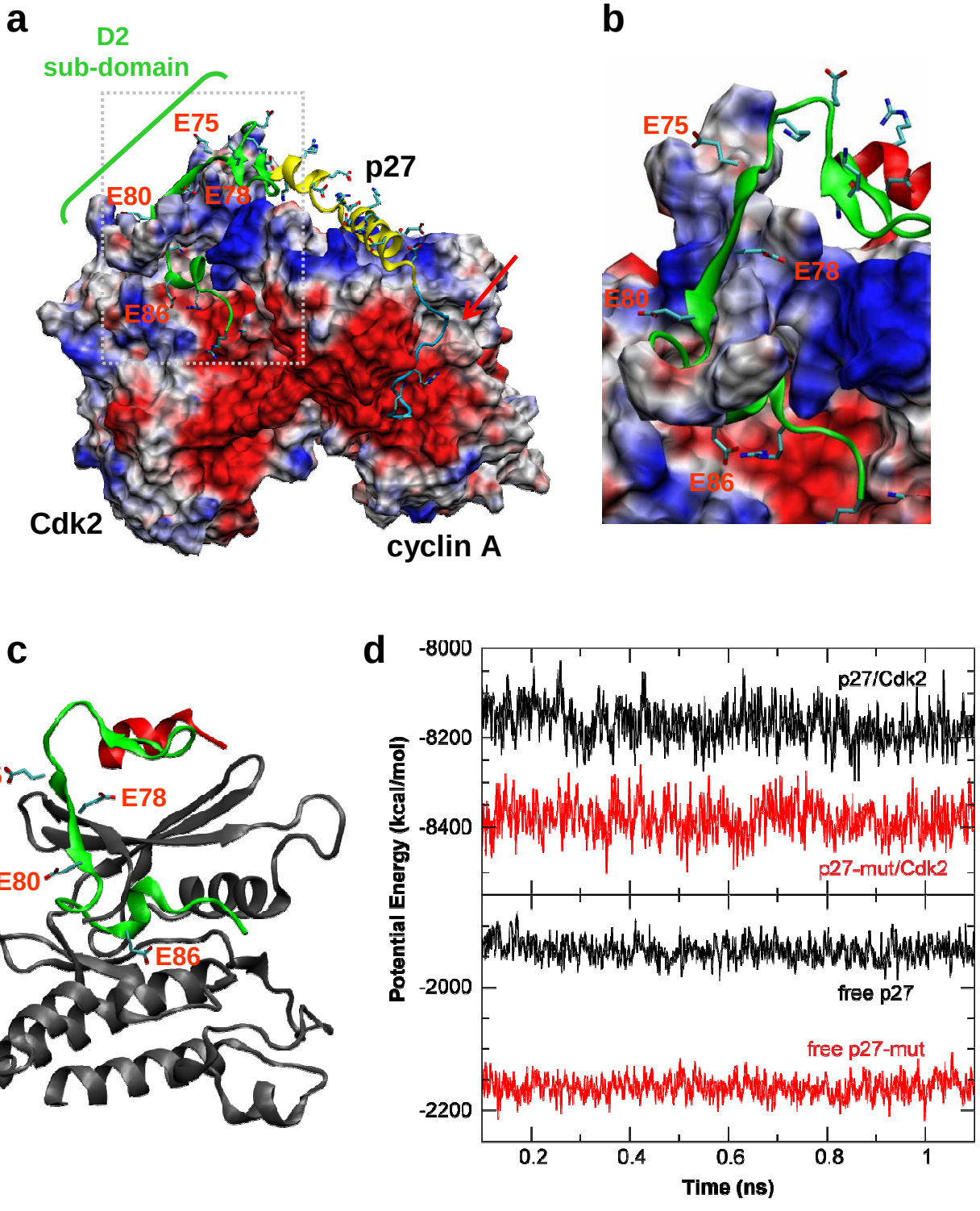

Supplementary Figure 5

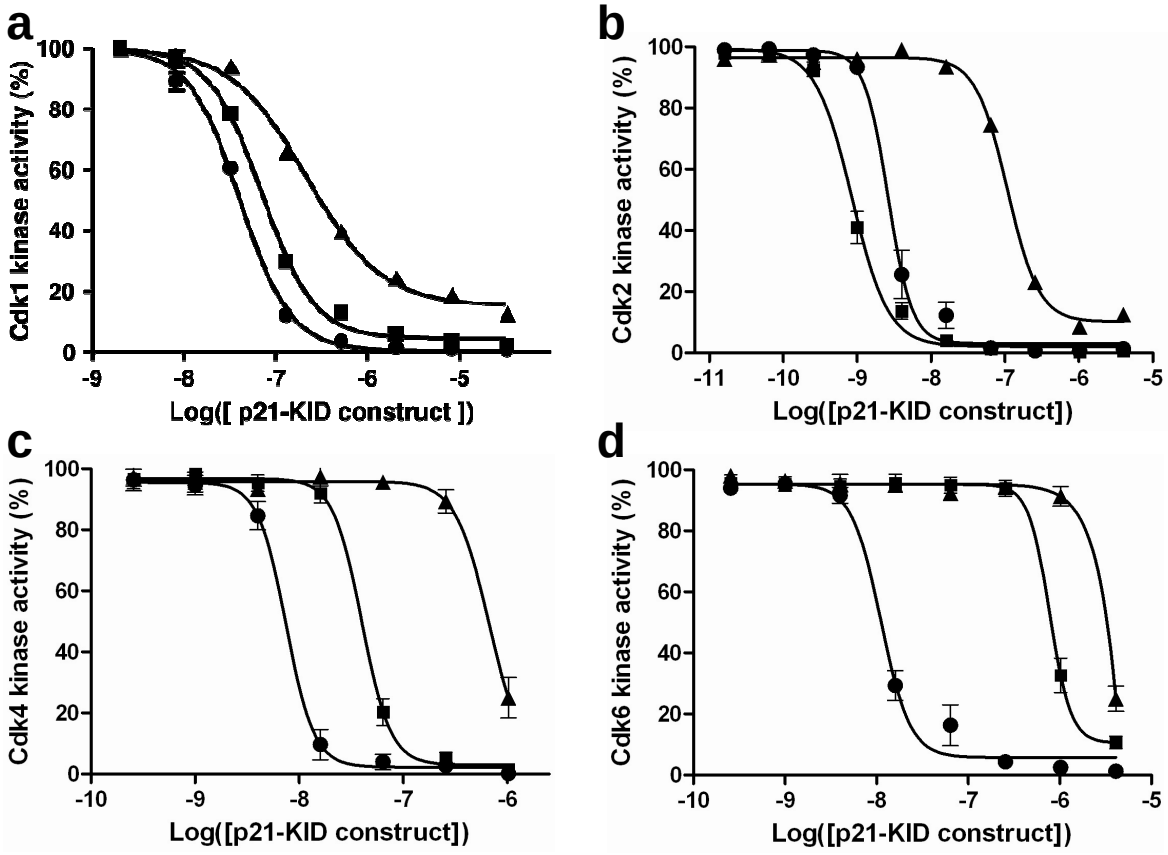

e

Cdk/cyclin complex	IC_{50} (nM)		
	p21-KID-LH_{-3}	p21-KID	p21-KID-LH_{+3}
Cdk1/cyclin B1	218 ± 29 [1]	40 ± 4	71 ± 7
Cdk2/cyclin A	108 ± 6	2.6 ± 0.2	0.8 ± 0.05
Cdk4/cyclin D1	680 ± 60	7.5 ± 0.7	40 ± 4
Cdk6/cyclin D1	2800 ± 200	11 ± 1	780 ± 100

[1] Cdk1/cyclin B1 was inhibited only to the extent of ~80%; the reported IC_{50} value corresponds to the midpoint of the partial inhibition curve.

Supplementary Figure 6

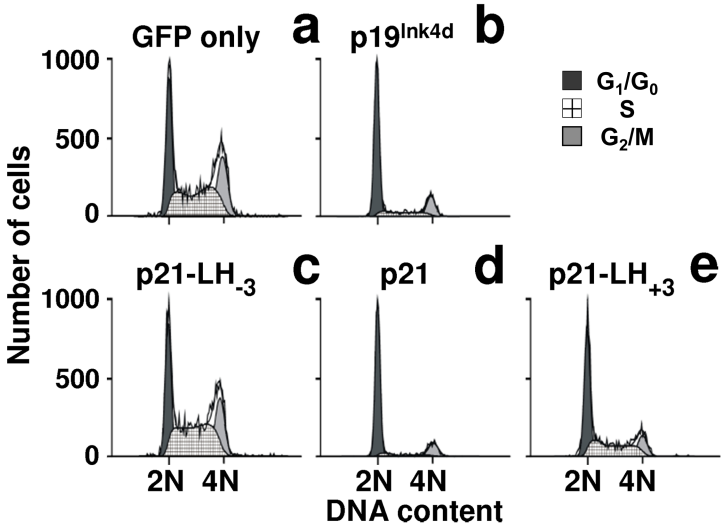

Supplementary Figure 7

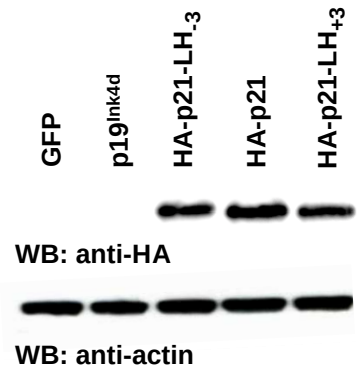

Supplementary Figure 8

Full-size versions of gel images illustrated in Supplementary Fig. 7

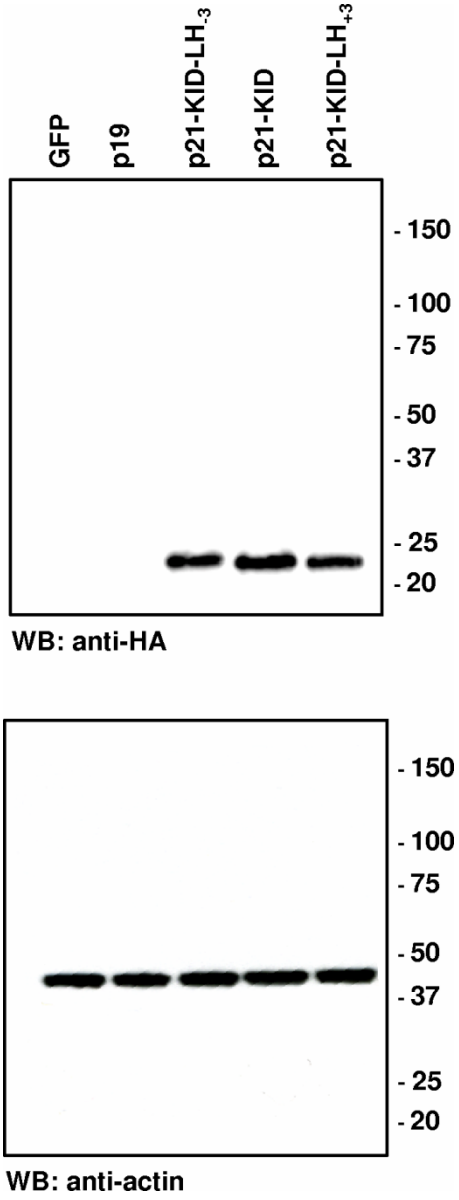

Supplementary Figure 9

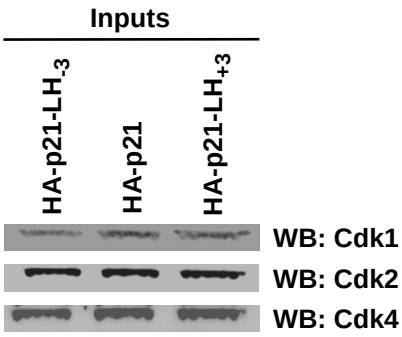

Supplementary Figure 10

Full-size versions of gel images illustrated in Fig. 4b

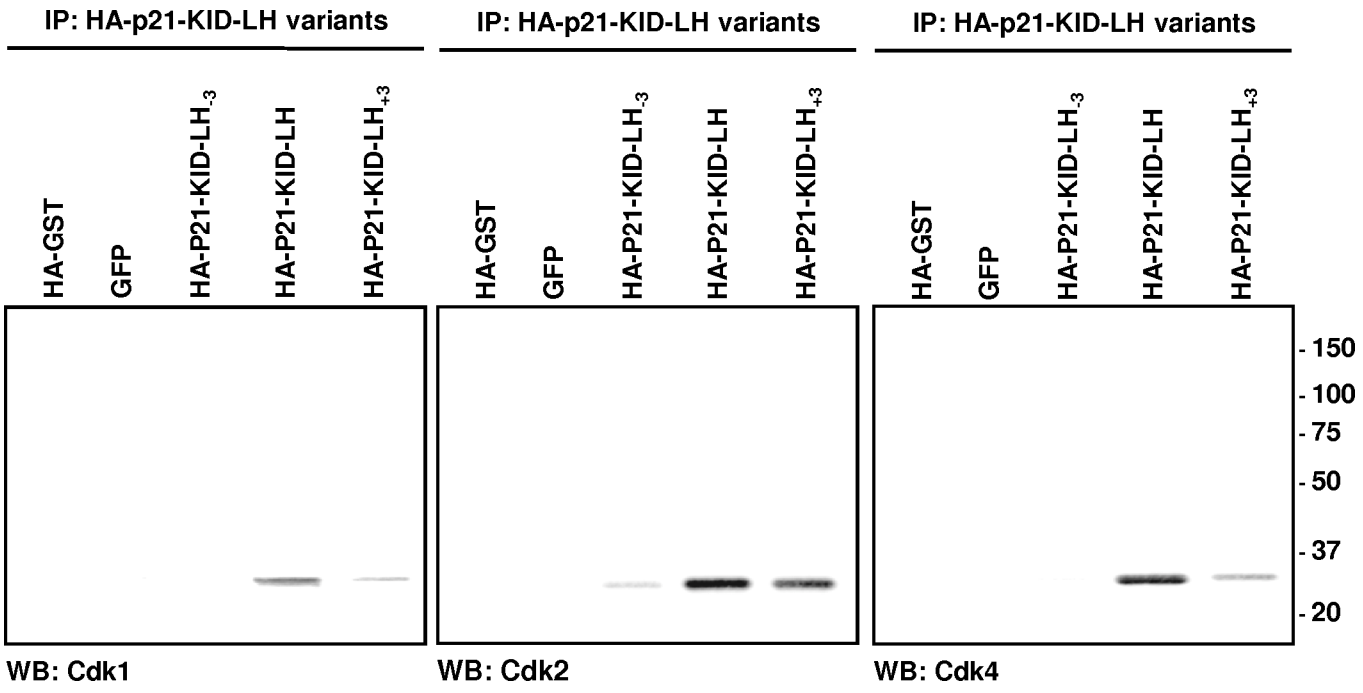

Supplementary Figure 11

Full-size version of gel image illustrated in Fig. 4c